

# Relic Density of Asymmetric Dark Matter with Sommerfeld enhancement

Aihemaitijiang Abudurusuli, Hoernisa Iminniyaz

*School of Physics Science and Technology, Xinjiang University,  
Urumqi 830046, China*

## Abstract

We investigate the evolution of abundance of the asymmetric thermal Dark Matter when its annihilation rate at chemical decoupling is boosted by the Sommerfeld enhancement. Then we discuss the effect of kinetic decoupling on relic abundance of asymmetric Dark Matter when the interaction rate depends on the velocity. Usually the relic density of asymmetric Dark Matter is analyzed in the frame of chemical decoupling. Indeed after decoupling from the chemical equilibrium, asymmetric Dark Matter particles and anti-particles were still in kinetic equilibrium for a while. It has no effect on the case of  $s$ -wave annihilation since there is no temperature dependence in this case. However, the kinetic decoupling has impacts for the case of  $p$ -wave annihilation and Sommerfeld enhanced  $s$ - and  $p$ -wave annihilations. We investigate in which extent the kinetic decoupling affects the relic abundances of asymmetric Dark Matter particle and anti-particle in detail. We found the constraints on the cross section and asymmetry factor by using the observational data of relic density of Dark Matter.

# 1 Introduction

There are compelling evidences for the existence of Dark Matter from the astrophysical and cosmological observations. Despite this evidences, the nature of Dark Matter is not made clear until now. Asymmetric Dark Matter is one of the alternatives which is contrary to the common assumption that the Majorana particle neutralino could be the candidate for Dark Matter which is Weakly Interacting Massive Stable Particles (WIMPs) appeared in supersymmetry. The idea for asymmetric Dark Matter arises from the possible link between the baryon number density and the Dark Matter energy density [1, 2]. The average density of baryons with  $\Omega_b = 0.046$  is comparable to that of Dark Matter. It is well known that the ordinary matter in the Universe is almost completely made from baryons, and the anti-baryons are contributing only a small fraction. The connection between the baryons and Dark Matter leads to the assumption that the Dark Matter particles can be asymmetric for which particles and antiparticles are not identical and there are more Dark Matter particles than antiparticles (or vice versa).

Refs.[3, 4] discussed the relic abundance of asymmetric Dark Matter in the standard cosmological scenario which assumed the asymmetric Dark Matter particles and anti-particles were in thermal equilibrium in the end of the radiation dominated era and decoupled when they become nonrelativistic. In this scenario, usually it is assumed the anti-particles are completely annihilated away with their particles and there are particles in the end. They showed that the final abundances of asymmetric Dark Matter particle and anti-particle are determined not only by the annihilation cross section, but also by the asymmetry factor which is the deviation of co-moving densities of the particle and anti-particle that is stated later in this paper.

In this work, we investigate the asymmetric Dark Matter which is coupled to the sufficiently light force mediators and the interaction between the Dark Matter particle and anti-particle appeared as long-range interaction. In this case, the wavefunction of asymmetric Dark Matter particle and antiparticle is distorted by the long-range interaction; it is the Sommerfeld effect [5]. The Sommerfeld effect enhances the late-time Dark Matter annihilation signals [6, 7]. The Sommerfeld enhancement is determined by the coupling of Dark Matter to the light force mediator. Asymmetric Dark Matter needs stronger couplings than the symmetric Dark Matter of the same mass, then the implications of the Sommerfeld enhancement for the phenomenology of asymmetric Dark Matter may be quite important than the symmetric Dark Matter case.

The effect of Sommerfeld enhancement on the relic density for symmetric Dark Matter was already investigated in [8, 9, 10, 11, 12, 13, 14]. In refs.[15, 16, 17, 18], the authors discussed asymmetric thermal Dark Matter with Sommerfeld enhancement including the effect

of the bound state. In this paper, we explore the relic density of asymmetric Dark Matter particles and anti-particles when the annihilation cross section of asymmetric Dark Matter particle and anti-particle is enhanced by the Sommerfeld effect. Here we only consider the Sommerfeld effect and neglect the effect of bound state formation on the relic density of asymmetric Dark Matter. We found the particle abundance is not modified significantly when the annihilation rate is boosted by Sommerfeld enhancement. However, for Dark Matter anti-particle, the decrease of abundance is more sizable than the case of without including the effect of Sommerfeld enhancement.

Although the asymmetric Dark Matter particles and anti-particles dropped out of chemical equilibrium, they were still in kinetic equilibrium for a while through the scattering off relativistic standard model particles in the thermal plasma. When the annihilating asymmetric Dark Matter particles and anti-particles were both in chemical and kinetic equilibrium, the temperatures of them tracks the background radiation temperature  $T$ , i.e.  $T_{\chi, \bar{\chi}} = T$ . At some point, the rate of scattering falls below the expansion rate of the universe, then the asymmetric Dark Matter particles and anti-particles dropped out of kinetic equilibrium. After kinetic decoupling, the temperatures of asymmetric Dark Matter particle and anti-particle are related by  $T_{\chi, \bar{\chi}} = T^2/T_k$  with the background radiation temperature  $T$ , where  $T_k$  is the kinetic decoupling temperature [19, 20]. The thermal average of cross section which is appeared in the Boltzmann equation is different before and after kinetic decoupling due to the change of temperature dependence. This has impacts on the relic densities of asymmetric Dark Matter particles and anti-particles. Without Sommerfeld enhancement, the kinetic decoupling has no effect on the relic abundance of asymmetric Dark Matter for  $s$ -wave annihilation since there is no temperature dependency in this case. However, there is very small impact in the case of  $p$ -wave annihilation. On the other hand, the effect is more significant both for the Sommerfeld enhanced  $s$ -wave and  $p$ -wave annihilations. The relic abundance of asymmetric Dark Matter is continuously decreased until the Sommerfeld enhancement ceases to have impact on the relic abundances.

The effect of kinetic decoupling on relic density of Dark Matter for the Sommerfeld enhancement was probed in refs.[11, 21, 22, 23]. Ref.[24] discussed the case including effect of resonance for  $m_\phi \neq 0$ . The impact of early kinetic decoupling on the relic density was also investigated in ref.[25]. In this work, we extend this discussion to the asymmetric Dark Matter. We explore the effects of kinetic decoupling on relic abundances of asymmetric Dark Matter particle and anti-particle in detail when the annihilation cross section of asymmetric Dark Matter is changed by Sommerfeld enhancement. Here we discuss the case where the mediator between asymmetric Dark Matter is massless,  $m_\phi = 0$ . We found the relic abundances of asymmetric Dark Matter particle and anti-particle are decreased after kinetic decoupling.

The decrease is almost invisible for asymmetric Dark Matter particle; on the other hand, the decrease is sizable for asymmetric Dark Matter anti-particle. The magnitude of the decrease depends on the asymmetry factor  $\eta$ , coupling strength  $\alpha$  and the kinetic decoupling temperature  $T_k$ .

The paper is arranged as following. In section 2, we discuss the thermal average of the Sommerfeld enhanced annihilation cross section for asymmetric Dark Matter. In Section 3, we study the numerical solution of asymmetric Dark Matter abundance including the effect of Sommerfeld enhancement. The analytic result for the relic density of asymmetric Dark matter is presented in section 4. In section 5, we investigate the effects of kinetic decoupling on the relic abundances of asymmetric Dark Matter particle and anti-particle. In section 6, the constraints on the parameter space are obtained by using the observational data of Dark Matter. In the last section, we summarize our results.

## 2 Sommerfeld enhanced annihilation cross section

For a massless light force carrier  $m_\phi$  (in the limit  $m_\phi \rightarrow 0$ ), the Sommerfeld factor for  $s$ -wave annihilation is

$$S_s = \frac{2\pi\alpha/v}{1 - e^{-2\pi\alpha/v}}, \quad (1)$$

and for  $p$ -wave annihilation

$$S_p = \left[1 + \left(\frac{\alpha}{v}\right)^2\right] \frac{2\pi\alpha/v}{1 - e^{-2\pi\alpha/v}}, \quad (2)$$

where  $v$  is the relative velocity of two annihilating asymmetric Dark Matter particle and anti-particle,  $\alpha$  is a coupling strength [26]. Here we only consider the annihilation of particle  $\chi$  and anti-particle  $\bar{\chi}$ . When the asymmetric Dark Matter particles and antiparticles decouple from the thermal background, they are nonrelativistic. Without Sommerfeld enhancement, the annihilation cross section for asymmetric Dark Matter particle and antiparticle can be expanded with respect to the relative velocity  $v$ ,

$$\langle\sigma v\rangle = a + b\langle v^2\rangle + \mathcal{O}(\langle v^4\rangle), \quad (3)$$

where  $a$  is the  $s$ -wave contribution to  $\sigma v$  when  $p$ -wave is suppressed,  $b$  describes the  $p$ -wave contribution to  $\sigma v$ . After including Sommerfeld enhancement on the thermal average of annihilation cross section, we have

$$\langle\sigma v\rangle_S = a\langle S_s\rangle + b\langle v^2 S_p\rangle + \mathcal{O}(v^4). \quad (4)$$

Here we use  $B_s$  and  $B_p$  to denote the Sommerfeld boost factors as

$$B_s = \langle S_s\rangle = \frac{x^{3/2}}{2\sqrt{\pi}} \int_0^\infty dv \, v^2 e^{-\frac{x}{4}v^2} \frac{2\pi\alpha/v}{1 - e^{-2\pi\alpha/v}}, \quad (5)$$

and

$$B_p = \langle v^2 S_p \rangle = \frac{x^{3/2}}{2\sqrt{\pi}} \int_0^\infty dv v^4 e^{-\frac{x}{4}v^2} \left[ 1 + \left(\frac{\alpha}{v}\right)^2 \right] \frac{2\pi\alpha/v}{1 - e^{-2\pi\alpha/v}}. \quad (6)$$

Where  $x = m/T$  with  $m$  being the mass of asymmetric Dark Matter. Following we obtain the analytic result of thermal average of Sommerfeld enhanced annihilation cross section times relative velocity in approximate way [14]. For the case,  $\pi\alpha/v \ll 1$ , we expand the factor  $(2\pi\alpha/v)/(1 - e^{-2\pi\alpha/v})$  in Eqs. (5,6) in Taylor series up to the second order,

$$\frac{2\pi\alpha/v}{1 - e^{-2\pi\alpha/v}} = 1 + \frac{\pi\alpha}{v} + \frac{1}{3}\left(\frac{\pi\alpha}{v}\right)^2. \quad (7)$$

Plugging the Taylor series into Eq.(4), we obtain

$$\begin{aligned} \langle \sigma v \rangle_{S,\text{Taylor}} &= a \left( 1 + \alpha\sqrt{\pi x} + \frac{1}{6}\pi^2\alpha^2 x \right) \\ &+ b \left[ \alpha^2 \left( 1 + \alpha\sqrt{\pi x} + \frac{1}{6}\pi^2\alpha^2 x \right) + \frac{6}{x} \left( 1 + \frac{2}{3}\alpha\sqrt{\pi x} + \frac{1}{18}\pi^2\alpha^2 x \right) \right]. \end{aligned} \quad (8)$$

When  $\alpha = 0$ , the standard annihilation cross section is recovered. In the opposite limit  $\pi\alpha/v \gg 1$ ,  $e^{-2\pi\alpha/v}$  in the denominator of Eqs.(5) and (6) are negligible, then the cross section is enhanced by  $1/v$ , we have

$$\langle \sigma v \rangle_{s,1/v} = 2\alpha\sqrt{\pi x}, \quad (9)$$

$$\langle \sigma v \rangle_{p,1/v} = 8\alpha\sqrt{\pi/x} + 2\alpha^3\sqrt{\pi x}. \quad (10)$$

Using Eq.(8) and applying Pade method, we can find the well fitting rational functions which connects the two limiting cases and can reproduce the exact numerical results for the thermal average of annihilation cross section times relative velocity,

$$\langle \sigma v \rangle_{S,\text{approx}} = a B_{s,\text{approx}} + b B_{p,\text{approx}}, \quad (11)$$

where

$$B_{s,\text{approx}} = \frac{1 + 7/4 \alpha\sqrt{\pi x} + 3/2 \alpha^2\pi x + (3/2 - \pi/3) (\alpha^2\pi x)^{3/2}}{1 + 3/4 \alpha\sqrt{\pi x} + (3/4 - \pi/6) \alpha^2\pi x}, \quad (12)$$

and

$$\begin{aligned} B_{p,\text{approx}} &= \alpha^2 \frac{1 + 7/4 \alpha\sqrt{\pi x} + 3/2 \alpha^2\pi x + (3/2 - \pi/3) (\alpha^2\pi x)^{3/2}}{1 + 3/4 \alpha\sqrt{\pi x} + (3/4 - \pi/6) \alpha^2\pi x} \\ &+ \frac{6}{x} \frac{1 + 4/3 \alpha\sqrt{\pi x} + (\pi + 4)/9 \alpha^2\pi x + 4/51 \pi (\alpha^2\pi x)^{3/2}}{1 + 2/3 \alpha\sqrt{\pi x} + \alpha^2\pi^2 x/18}. \end{aligned} \quad (13)$$

We noted that the choice is not unique. The approximation reproduces the exact results with accuracy of less than 0.5%.

Fig.1 shows the ratio of exact values of thermally averaged Sommerfeld boost factors  $B_s$ ,  $B_p$  and the approximation of  $B_{s,\text{approx}}$ ,  $B_{p,\text{approx}}$  as a function of  $\alpha$  for the typical inverse-scaled WIMP decoupling temperature  $m/T = 22$  in (a) and (b). We found that our approximation reproduce the exact results with accuracy of less than 0.5% in both (a) and (b).

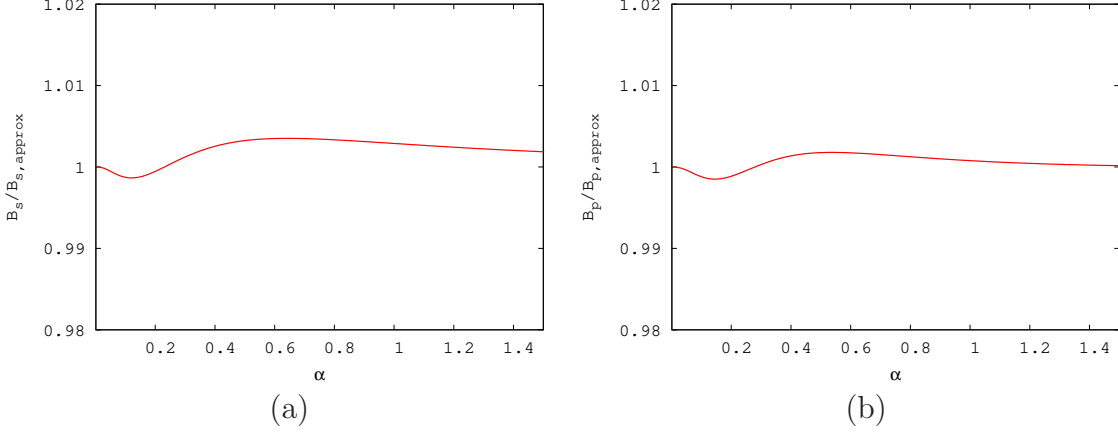


Figure 1: The ratio of the exact value of  $B_s$  ( $B_p$ ) and the approximation of  $B_{s,approx}$  ( $B_{p,approx}$ ) as a function of  $\alpha$  for  $m/T = 22$  in (a) ((b)).

### 3 Numerical solution of the abundance of asymmetric Dark Matter including Sommerfeld enhancement

After including Sommerfeld enhanced annihilation cross section in the Boltzmann equation which describes the evolution of number densities of asymmetric Dark Matter particle and anti-particle, we have

$$\frac{dn_{\chi,\bar{\chi}}}{dt} + 3Hn_{\chi,\bar{\chi}} = -\langle\sigma v\rangle_S(n_{\chi}n_{\bar{\chi}} - n_{\chi,eq}n_{\bar{\chi},eq}), \quad (14)$$

where  $\chi$  is for particle and  $\bar{\chi}$  for anti-particle and the expansion rate in the radiation dominated era,  $H = \pi T^2/M_{Pl} \sqrt{g_*/90}$ , here  $M_{Pl} = 2.4 \times 10^{18}$  GeV is the reduced Planck mass, with  $g_*$  being the effective number of relativistic degrees of freedom. The equilibrium number densities are  $n_{\chi,eq} = g_{\chi} [mT/(2\pi)]^{3/2} e^{(-m+\mu_{\chi})/T}$  and  $n_{\bar{\chi},eq} = g_{\chi} [mT/(2\pi)]^{3/2} e^{(-m-\mu_{\chi})/T}$ . Here the chemical potentials  $\mu_{\chi}$ ,  $\mu_{\bar{\chi}}$  for  $\chi$  and  $\bar{\chi}$  are equal when the asymmetric Dark Matter particle  $\chi$  and anti-particle  $\bar{\chi}$  are in equilibrium,  $\mu_{\bar{\chi}} = -\mu_{\chi}$ , where  $g_{\chi}$  is the number of intrinsic degrees of freedom of the particle.

The Boltzmann equation in terms of the ratio of number densities of particle and anti-particle to entropy density  $Y_{\chi,\bar{\chi}} = n_{\chi,\bar{\chi}}/s$ , and  $x$ , is

$$\frac{dY_{\chi,\bar{\chi}}}{dx} = -\frac{\lambda\langle\sigma v\rangle_S}{x^2} (Y_{\chi} Y_{\bar{\chi}} - Y_{\chi,eq} Y_{\bar{\chi},eq}), \quad (15)$$

where  $s = 2\pi^2 g_{*s}/45 T^3$ , with  $g_{*s}$  being the effective number of entropic degrees of freedom. Here we used the entropy conservation,  $\lambda = 1.32 m M_{Pl} \sqrt{g_*}$ ,  $g_* \simeq g_{*s}$  and  $dg_{*s}/dx \simeq 0$ . The subtraction of the Boltzmann equations for  $\chi$  and  $\bar{\chi}$  results

$$\frac{dY_{\chi}}{dx} - \frac{dY_{\bar{\chi}}}{dx} = 0. \quad (16)$$

This means

$$Y_\chi - Y_{\bar{\chi}} = \eta, \quad (17)$$

where  $\eta$  is a constant, the difference of the co-moving densities of the particles and anti-particles is conserved. Inserting this into Boltzmann equation (15), then

$$\frac{dY_\chi}{dx} = -\frac{\lambda\langle\sigma v\rangle_S}{x^2} (Y_\chi^2 - \eta Y_\chi - Y_{\text{eq}}^2), \quad (18)$$

$$\frac{dY_{\bar{\chi}}}{dx} = -\frac{\lambda\langle\sigma v\rangle_S}{x^2} (Y_{\bar{\chi}}^2 + \eta Y_{\bar{\chi}} - Y_{\text{eq}}^2), \quad (19)$$

here  $Y_{\text{eq}}^2 = Y_{\chi,\text{eq}}Y_{\bar{\chi},\text{eq}} = (0.145g_\chi/g_*)^2 x^3 e^{-2x}$ . We noted that  $Y_{\text{eq}}^2$  doesn't depend on the chemical potential  $\mu_\chi$ .

In the standard picture of particle evolution scenarios, it is assumed the asymmetric Dark Matter particles and anti-particles were in thermal equilibrium with the standard model plasma in the early universe. They decoupled from equilibrium whenever the interaction rate  $\Gamma$  drops below the expansion rate  $H$ . At this point the temperature is less than the mass of asymmetric Dark Matter particles,  $T < m$  for  $m > |\mu_\chi|$  [3, 4, 27]. This is the freeze out temperature at which point the number densities of asymmetric Dark Matter particle and anti-particle in a co-moving space almost become constant.

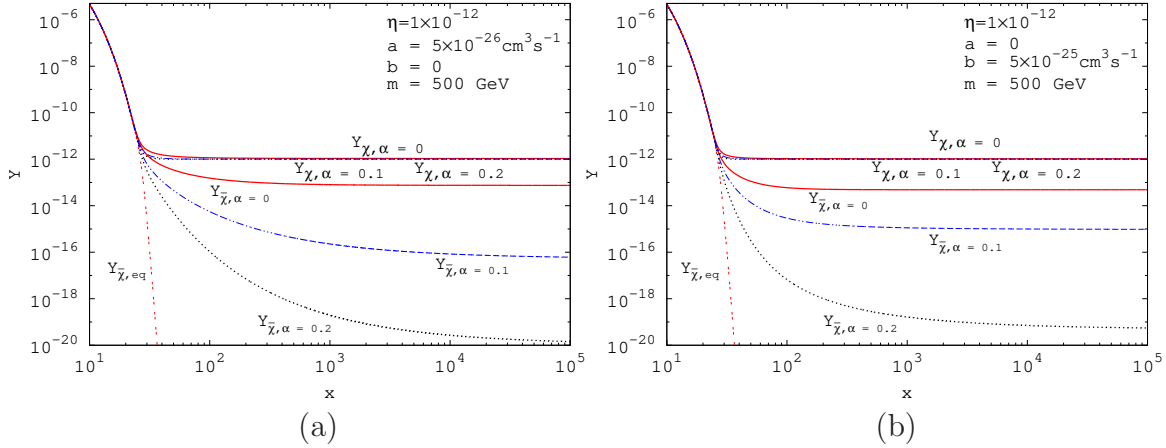


Figure 2: Evolution of  $Y$  for the particle and anti-particle as a function of  $x$  for the case when the annihilation cross section is boosted by Sommerfeld enhancement and without enhancement. Here  $g_\chi = 2$ ,  $g_* = 90$ .

Fig.2 shows the evolution of abundances of Dark Matter particle and anti-particle when the annihilation cross section is enhanced by Sommerfeld effect. It is plotted using the numerical solutions of equations (18), (19). In panel (a), the thick (red) lines are for relic abundances  $Y_\chi$  and  $Y_{\bar{\chi}}$  for asymmetric Dark Matter particle and anti-particle without Sommerfeld effect. The dashed (blue) lines are for the case of Sommerfeld factor  $\alpha = 0.1$  and dotted (black) lines are for the case of Sommerfeld factor  $\alpha = 0.2$ . The double dotted (red) is for the

equilibrium value of anti-particle abundance. It is shown that deviations between the particle abundances of the case with Sommerfeld enhancement and without are very small for the case of  $\alpha = 0.1$  and  $\alpha = 0.2$ . We found that the particle abundance is not affected appreciably comparing to the anti-particle abundance. The impact of Sommerfeld enhancement on relic abundance of anti-particle is more significant when the Sommerfeld factor  $\alpha$  is larger. The similar results is obtained for the case of  $p$ -wave annihilation in plot (b). The asymmetric Dark Matter decouples later due to the boosted annihilation rate comparing to the case without Sommerfeld enhancement, and hence the relic abundances for particle and anti-particle are decreased in principle. For  $\alpha = 0.1$  and  $\alpha = 0.2$  in Fig.2, the decreases of anti-particle abundances are few orders less than  $\eta$ , then the particle abundances kept in the same order of  $\eta$  due to the relation  $Y_\chi - Y_{\bar{\chi}} = \eta$ , because the anti-particle abundance is too small to alter the particle abundance in Eq.(17). This is the reason why the particle abundance is not changed sizably comparing to the anti-particle abundance. For the smaller value of  $\eta$ , as in Fig.3, the decrease of asymmetric Dark Matter particle abundance is obvious.

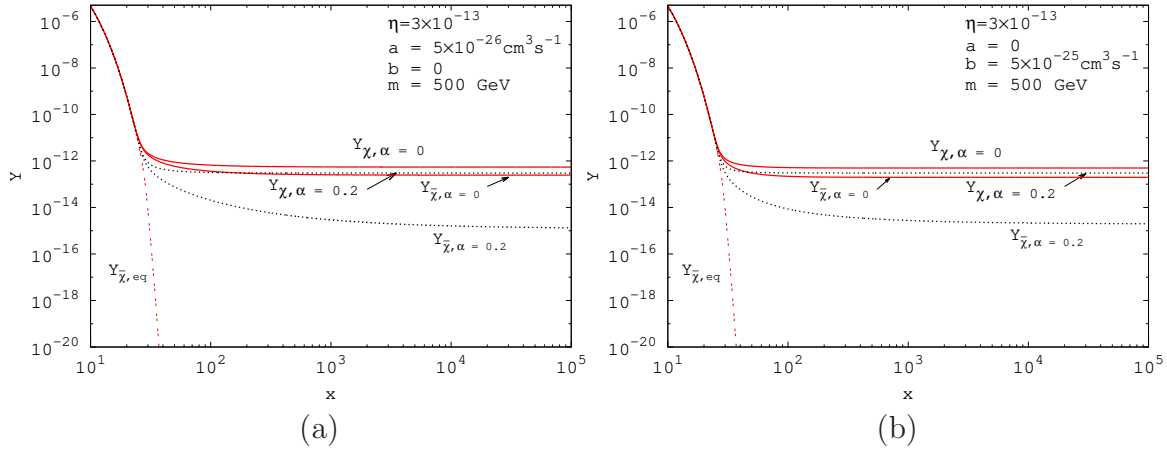


Figure 3: Evolution of  $Y$  for the particle and anti-particle as a function of  $x$  for the case when the annihilation cross section is boosted by Sommerfeld enhancement and without enhancement. Here  $g_\chi = 2$ ,  $g_* = 90$ .

## 4 Analytical solutions

We follow the method which is used in [3, 4] to find the analytic solution, we first write the Boltzmann equation (19) in terms of  $\Delta_{\bar{\chi}} = Y_{\bar{\chi}} - Y_{\bar{\chi},\text{eq}}$ ,

$$\frac{d\Delta_{\bar{\chi}}}{dx} = -\frac{dY_{\bar{\chi},\text{eq}}}{dx} - \frac{\lambda\langle\sigma v\rangle_S}{x^2} [\Delta_{\bar{\chi}}(\Delta_{\bar{\chi}} + 2Y_{\bar{\chi},\text{eq}}) + \eta\Delta_{\bar{\chi}}] . \quad (20)$$



For high temperature,  $Y_{\bar{\chi}} \sim Y_{\bar{\chi},\text{eq}}$ , therefore we ignore  $\Delta_{\bar{\chi}}^2$  and  $d\Delta_{\bar{\chi}}/dx$ , then

$$\Delta_{\bar{\chi}} \simeq \frac{2x^2 Y_{\text{eq}}^2}{\lambda \langle \sigma v \rangle_S (\eta^2 + 4Y_{\text{eq}}^2)}, \quad (21)$$

here  $Y_{\bar{\chi},\text{eq}} = -\eta/2 + \sqrt{\eta^2/4 + Y_{\text{eq}}^2}$ , which is obtained by solving the Boltzmann equation (19) in equilibrium state. Eq.(21) is used to fix the freeze out temperature  $\bar{x}_F$  for  $\bar{\chi}$ .

At late time, when the temperature is low,  $x > \bar{x}_F$ , the equilibrium value of relic abundance  $Y_{\bar{\chi},\text{eq}}$  is negligible. Thus after dropping the term which is related to  $Y_{\bar{\chi},\text{eq}}$  in Eq.(20), we have

$$\frac{d\Delta_{\bar{\chi}}}{dx} = -\frac{\lambda \langle \sigma v \rangle_S}{x^2} (\Delta_{\bar{\chi}}^2 + \eta \Delta_{\bar{\chi}}), \quad (22)$$

here we assume that  $\Delta_{\bar{\chi}}(\bar{x}_F) \gg \Delta_{\bar{\chi}}(x_\infty)$  and integrate Eq.(22) from  $\bar{x}_F$  to  $\infty$ , then

$$Y_{\bar{\chi}}(x_\infty) = \eta \left\{ \exp \left[ 1.32 \eta m M_{\text{Pl}} \sqrt{g_*} \int_{\bar{x}_F}^{\infty} \frac{\langle \sigma v \rangle_S}{x^2} dx \right] - 1 \right\}^{-1}, \quad (23)$$

where

$$\begin{aligned} \int_{\bar{x}_F}^{\infty} \frac{\langle \sigma v \rangle_S}{x^2} dx &= (a + \alpha^2 b) \left[ \frac{1}{\bar{x}_F} + 2\alpha \sqrt{\frac{\pi}{\bar{x}_F}} + \frac{\pi^2 \alpha^2}{6} \ln \left( 1 + \frac{9\alpha \sqrt{\pi \bar{x}_F} + 12}{(9 - 2\pi)\pi \alpha^2 \bar{x}_F} \right) \right. \\ &+ \left. \pi \alpha^2 \frac{36 - 11\pi}{\sqrt{3(117 - 32\pi)}} \left( \frac{\pi}{2} - \tan^{-1} \frac{2(9 - 2\pi)\alpha \sqrt{\pi \bar{x}_F} + 9}{\sqrt{3(117 - 32\pi)}} \right) \right] \\ &+ b \left[ \frac{3}{\bar{x}_F^2} + \frac{8\sqrt{\pi}\alpha}{3\bar{x}_F^{3/2}} + \frac{\pi^2 \alpha^2}{3\bar{x}_F} + \frac{8\pi^{5/2} \alpha^3}{153\sqrt{\bar{x}_F}} + \frac{(16 + 13\pi)\pi^3 \alpha^4}{459\sqrt{\pi/2 - 1}} \left( \frac{\pi}{2} - \tan^{-1} \frac{6 + \pi^{3/2} \alpha \sqrt{\bar{x}_F}}{3\sqrt{2(\pi - 2)}} \right) \right. \\ &- \left. \frac{(16 + 17\pi)\pi^3 \alpha^4}{918} \ln \left( 1 + \frac{12}{\pi \alpha \sqrt{\pi \bar{x}_F}} + \frac{18}{\pi^2 \alpha^2 \bar{x}_F} \right) \right]. \end{aligned} \quad (24)$$

The relic abundance for  $\chi$  particle is obtained by using Eq.(17),

$$Y_{\chi}(x_\infty) = \eta \left\{ 1 - \exp \left[ -1.32 \eta m M_{\text{Pl}} \sqrt{g_*} \int_{x_F}^{\infty} \frac{\langle \sigma v \rangle_S}{x^2} dx \right] \right\}^{-1}, \quad (25)$$

where  $x_F$  is the freeze out temperature for  $\chi$ . Eqs.(23) and (25) are only consistent with constraint (17) if  $x_F = \bar{x}_F$ . The total final Dark Matter relic density is

$$\Omega_{\text{DM}} h^2 = 2.76 \times 10^8 [Y_{\chi}(x_\infty) + Y_{\bar{\chi}}(x_\infty)] m, \quad (26)$$

where we used  $\Omega_{\chi} = \rho_{\chi}/\rho_c$  with  $\rho_{\chi} = n_{\chi} m = s_0 Y_{\chi}$  and  $\rho_c = 3H_0^2 M_{\text{Pl}}^2$ , here  $s_0 \simeq 2900 \text{ cm}^{-3}$  is the present entropy density, and  $H_0$  is the Hubble constant. We use the equality,  $\xi Y_{\bar{\chi},\text{eq}}(\bar{x}_F) = \Delta_{\bar{\chi}}(\bar{x}_F)$ , to fix the freezing out temperature, here  $\xi$  is a constant, usually we take  $\xi = \sqrt{2} - 1$  [27]. We found the analytic result matches with the numerical result within the accuracy of 10%.

## 5 Effects of kinetic decoupling on the relic abundance of asymmetric Dark Matter

The effects of Sommerfeld enhancement on the relic density of asymmetric Dark Matter is analyzed in the previous section. It was assumed the temperatures of annihilating asymmetric Dark Matter particles and anti-particles track the background radiation temperature  $T$  when the annihilating asymmetric Dark Matter particles and anti-particles remains in chemical and kinetic equilibrium with the radiation background. During radiation dominated era, the temperature of radiation scales as  $T \propto 1/R$ , with  $R$  being the scale factor of the universe. Asymmetric Dark Matter particle and anti-particle are still in kinetic equilibrium after dropping out of chemical equilibrium. At some point  $T_k$ , asymmetric Dark Matter particles and anti-particles decouple from kinetic equilibrium and the temperature of asymmetric Dark Matter scales as  $T_{\chi, \bar{\chi}} \propto 1/R^2$  [19, 20, 28, 29]. The determination of precise value of the kinetic decoupling temperature  $T_k$  depends on the models. In supersymmetric models discussed in [20],  $T_k \approx (10^{-3} - 10^{-1})T_F$ . In this work, we take  $T_k/T_F$  as a free parameter for the generality with the constraint  $T_k < T_F$ . Then the relation between the temperatures of asymmetric Dark Matter  $T_{\chi, \bar{\chi}}$  and the radiation temperature  $T$  is [19, 20]

$$T_{\chi, \bar{\chi}} = \frac{T^2}{T_k}. \quad (27)$$

This change will affect the thermal average of the annihilation cross section between the asymmetric Dark Matter particle and anti-particle. For the case of  $s$ -wave annihilation, the cross section is independent of  $T_{\chi, \bar{\chi}}$ , therefore, kinetic decoupling has no effect on the relic density of asymmetric Dark Matter in this case. For the  $p$ -wave annihilation or Sommerfeld enhanced  $s$ - and  $p$ -wave annihilations, there are temperature dependencies of the annihilation cross section, then the relic density is affected by kinetic decoupling. After kinetic decoupling, thermal average of  $p$ -wave annihilation cross section becomes  $\langle \sigma v \rangle_p = 6b x_k/x^2$ . The Boltzmann equations of asymmetric Dark Matter anti-particle for  $p$ -wave annihilation before and after kinetic decoupling are

$$\frac{dY_{\bar{\chi}}}{dx} = -1.32 m M_{\text{Pl}} \sqrt{g_*} (6b x^{-3}) (Y_{\bar{\chi}}^2 + \eta Y_{\bar{\chi}} - Y_{\text{eq}}^2), \quad (28)$$

$$\frac{dY_{\bar{\chi}}}{dx} = -1.32 m M_{\text{Pl}} \sqrt{g_*} (6b x_k x^{-4}) (Y_{\bar{\chi}}^2 + \eta Y_{\bar{\chi}} - Y_{\text{eq}}^2), \quad (29)$$

The effects of kinetic decoupling on the final relic density of asymmetric Dark Matter for  $p$ -wave annihilation is estimated by integrating Boltzmann equation (28) from  $\bar{x}_F$  to  $x_k$  and equation (29) from  $x_k$  to  $\infty$ . When there is kinetic decoupling, we obtain the relic abundance

for asymmetric Dark Matter anti-particle for  $p$ -wave annihilation as

$$Y_{\bar{\chi}}(x_{\infty}) = \eta \left\{ \exp \left[ 1.32 \eta m M_{\text{Pl}} \sqrt{g_*} \left( \int_{x_F}^{x_k} \frac{6b}{x^3} dx + \int_{x_k}^{\infty} \frac{6bx_k}{x^4} dx \right) \right] - 1 \right\}^{-1}. \quad (30)$$

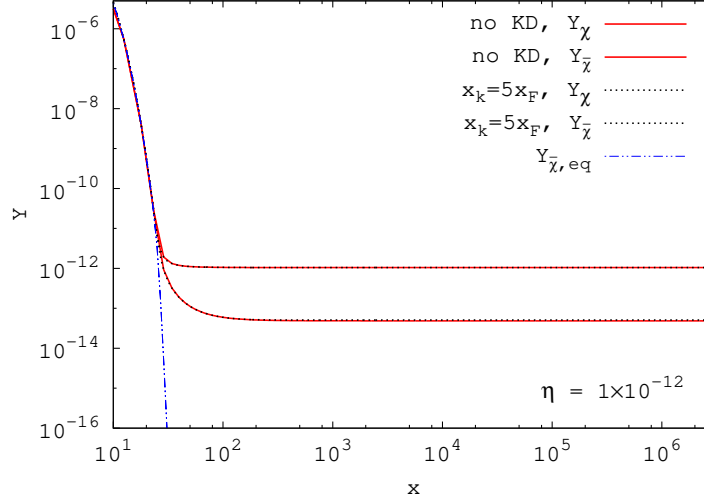


Figure 4: The effect of kinetic decoupling on the evolution of  $Y$  for the particle and anti-particle as a function of  $x$  for  $p$ -wave annihilation cross section. Here  $g_{\chi} = 2$ ,  $g_* = 90$ ,  $m = 500$  GeV,  $x_F = 25$ ,  $a = 0$ ,  $b = 5 \times 10^{-25} \text{ cm}^3 \text{ s}^{-1}$ ,  $\eta = 1 \times 10^{-12}$ .

In Fig.4, we plot the relic abundances of asymmetric Dark Matter particle  $Y_{\chi}$  and anti-particle  $Y_{\bar{\chi}}$  as a function of the inverse-scaled temperature  $x$  for  $p$ -wave annihilation cross section when the kinetic decoupling temperature  $x_k = 5x_F$ , here  $\alpha = 0$ ,  $a = 0$ ,  $b = 5 \times 10^{-25} \text{ cm}^3 \text{ s}^{-1}$ ,  $\eta = 1 \times 10^{-12}$  and  $m = 500$  GeV. The effects of kinetic decoupling on the asymmetric Dark Matter particle abundance  $Y_{\chi}$  and anti-particle abundance  $Y_{\bar{\chi}}$  are negligible when kinetic decoupling temperature  $x_k = 5x_F$ . The Dark Matter particle abundance is almost not changed after kinetic decoupling. The difference between the anti-particle abundance before and after kinetic decoupling is by a factor of 1. Because we are discussing the case where kinetic decoupling occurred after the asymmetric Dark Matter particles and anti-particles decoupled from chemical equilibrium, again here we assume the kinetic decoupling occurred at the point which is 5 times of inverse-scaled chemical decoupling temperature, therefore, the effect is negligible in this case. It may have significant effects if the kinetic decoupling occurs earlier. In that case, one must solve the coupled Boltzmann equations which we didn't consider in our work for simplicity [25].

The effect of kinetic decoupling is more noticeable for the case of Sommerfeld enhanced  $s$ -wave and  $p$ -wave annihilations. With the kinetic decoupling, the Sommerfeld enhanced

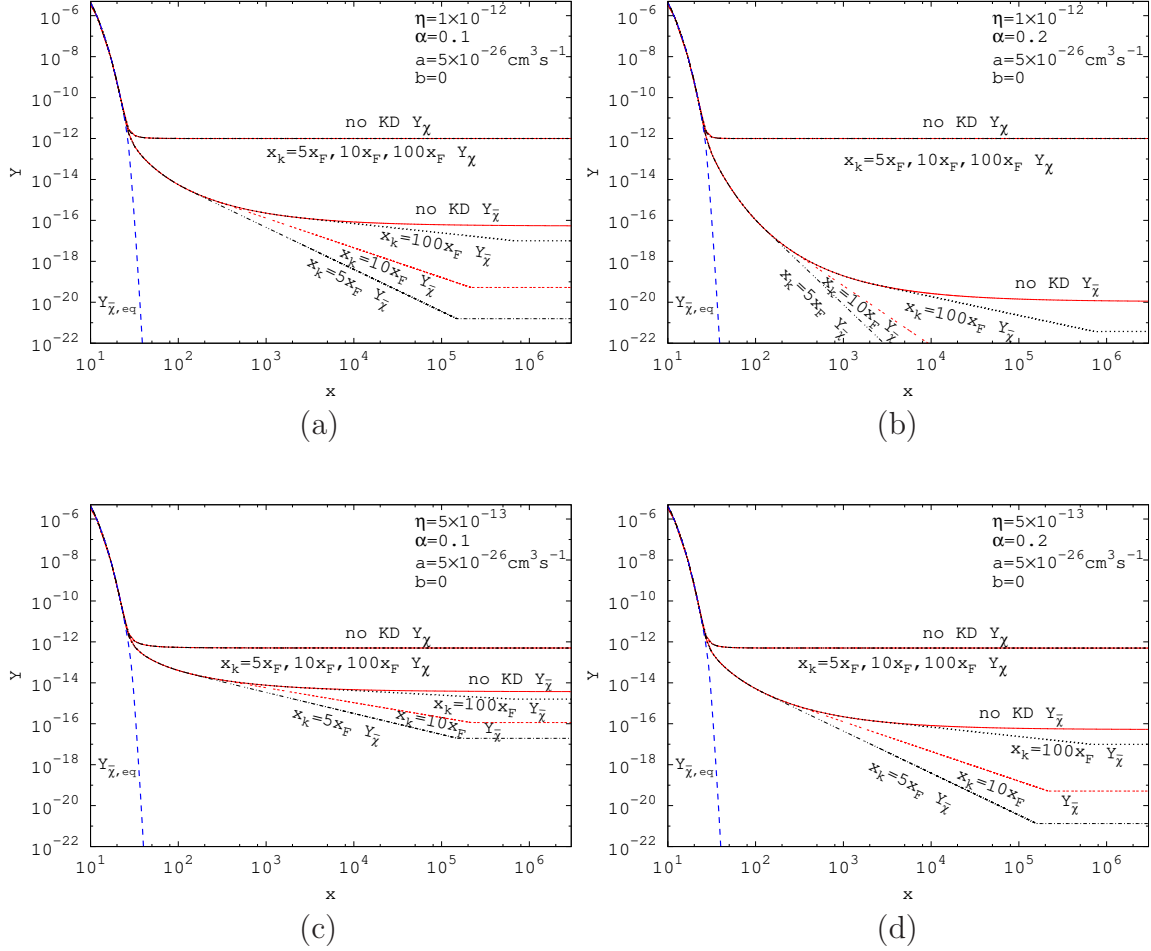


Figure 5: The effects of kinetic decoupling on the evolution of  $Y$  for asymmetric Dark Matter particle and anti-particle as a function of  $x$  for Sommerfeld enhanced  $s$ -wave annihilation cross section for different asymmetry factors and coupling strengths. Here  $g_\chi = 2$ ,  $g_* = 90$ ,  $m = 500$  GeV,  $x_F = 25$ .

annihilation cross sections become

$$\langle \sigma v \rangle_{S_k} \simeq \frac{x^3}{2\sqrt{\pi}x_k^3} \int_0^\infty dv e^{-\frac{x^2}{4x_k}v^2} \left\{ a v^2 \frac{2\pi\alpha/v}{1 - e^{-2\pi\alpha/v}} + b v^4 \left[ 1 + \left( \frac{\alpha}{v} \right)^2 \right] \frac{2\pi\alpha/v}{1 - e^{-2\pi\alpha/v}} \right\}. \quad (31)$$

Then the Boltzmann equation (19) of asymmetric Dark Matter anti-particle for Sommerfeld enhanced  $s$ - and  $p$ -wave annihilation cross sections is

$$\frac{dY_{\bar{\chi}}}{dx} = -1.32 m M_{\text{Pl}} \sqrt{g_*} \langle \sigma v \rangle_{S_k} x^{-2} (Y_{\bar{\chi}}^2 + \eta Y_{\bar{\chi}} - Y_{\text{eq}}^2), \quad (32)$$

Fig.5 shows the evolution of  $Y_\chi$  and  $Y_{\bar{\chi}}$  as a function of  $x$  for  $s$ -wave annihilation cross section when  $\alpha = 0.1$  in panels (a), (c) and  $\alpha = 0.2$  in panels (b), (d). Here the asymmetry factor  $\eta = 1 \times 10^{-12}$  in panels (a), (b);  $\eta = 5 \times 10^{-13}$  in (c), (d) and  $m = 500$  GeV,  $a = 5 \times 10^{-26} \text{ cm}^3 \text{ s}^{-1}$ ,  $b = 0$ . We plot the figure by using the numerical solution of Eq.(19) from the range of  $\bar{x}_F$  to  $x_k$  and Eq.(32) from  $x_k$  to quite large value of  $x$ , here we take

$x = 3 \times 10^6$ . We found the asymmetric Dark Matter particle abundances for different kinetic decoupling temperatures are almost same with the case that there is no kinetic decoupling. On the other hand, after kinetic decoupling, the relic abundances for anti-particle are decreased continuously until the annihilation becomes inefficient. If we replace  $x$  with  $x_\chi = x^2/x_k$  in the analytic result of the  $s$ -wave Sommerfeld factor in Eq.(12), the Sommerfeld factor  $\propto x$  for sufficiently large  $x$ . After the integration of equation (32), for large  $x$ , the anti-particle abundance for  $s$ -wave annihilation cross section scales as  $Y_{\bar{\chi}} \propto \eta/x^c$ , where  $c \propto 1.32\eta m M_{\text{Pl}} \sqrt{g_*} \alpha a$ , which is constant. It matches with the numerical result. However, this decrease will eventually be stopped by one of the following three effects [24]. One is that the Sommerfeld enhancement is saturated at low velocity, it works for the massive mediator case. Second is that the onset of matter domination. The last one is the onset of structure formation which finally eliminates the Sommerfeld effect. We use  $x_{\text{cut}}$  to express the point at which the Sommerfeld effect is eliminated. In plot (a), the relic abundances become constant around  $x_{\text{cut}} = 1.5 \times 10^5$  for  $x_k = 5x_F$ ,  $2.2 \times 10^5$  for  $x_k = 10x_F$  and  $6.9 \times 10^5$  for  $x_k = 100x_F$ . We obtained these points from the numerical data. The asymmetric Dark Matter annihilation rate is insignificant from that points and  $Y_{\bar{\chi}}$  becomes stable. The inverse-scaled temperature at which the annihilations become inefficient is important for the correct determination of the relic density of asymmetric Dark Matter. The decrease of abundance of Dark Matter anti-particle is larger when the decoupling temperature is more close to the chemical freezing out point  $x_F$ . The reduction is also more sizable for larger  $\alpha$ . For the smaller asymmetry factor  $\eta = 5 \times 10^{-13}$ , the decreases of Dark Matter anti-particle abundances are less than the case of  $\eta = 1 \times 10^{-12}$  which are shown in panels (c) and (d).

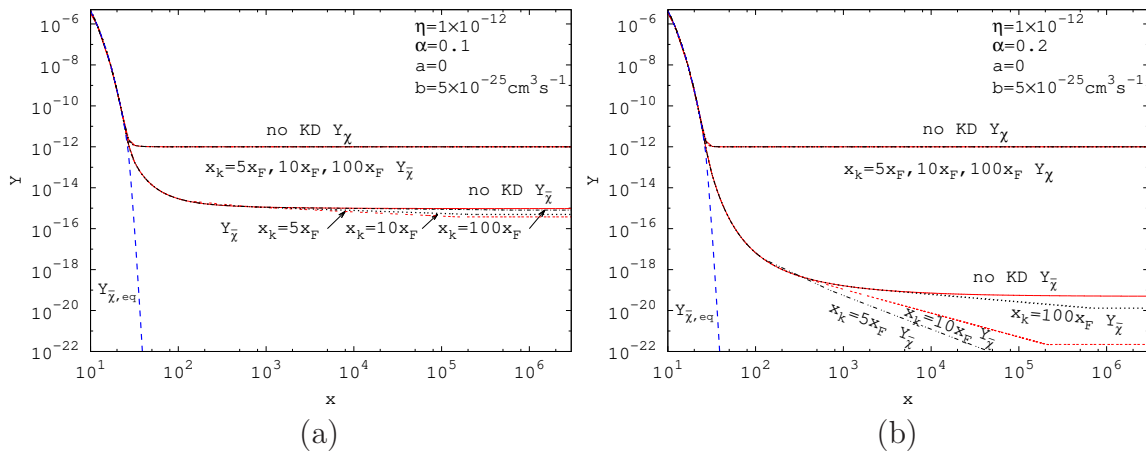


Figure 6: The effects of kinetic decoupling on the evolution of  $Y$  for the particle and anti-particle as a function of  $x$  for Sommerfeld enhanced  $p$ -wave annihilation cross section. Here  $g_\chi = 2$ ,  $g_* = 90$ ,  $m = 500$  GeV,  $x_F = 25$ .

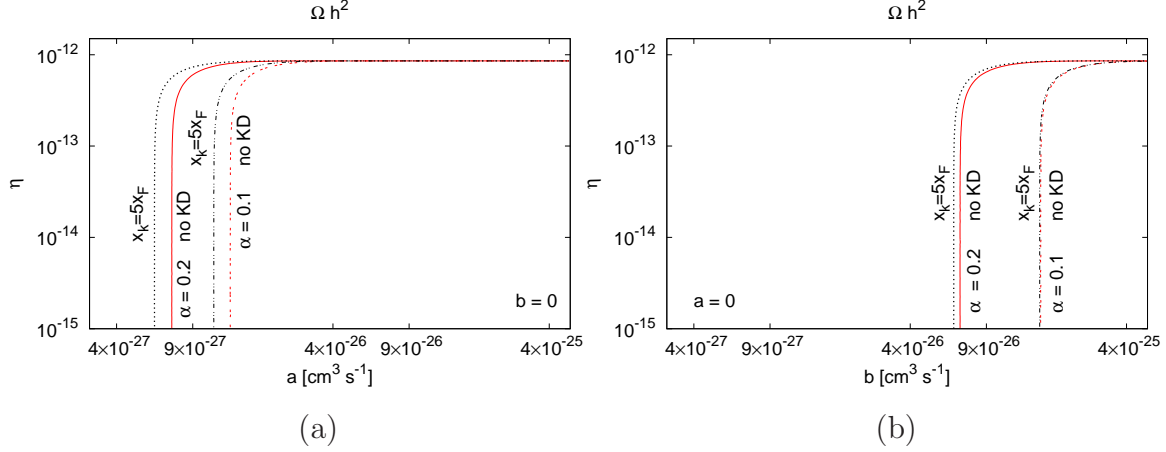


Figure 7: The contour plots of  $s$ - ( $b = 0$ ) and  $p$ -wave ( $a = 0$ ) annihilation cross sections and the asymmetry factor  $\eta$  when  $\Omega_{\text{DM}} h^2 = 0.1199$ . Here  $g_\chi = 2$ ,  $g_* = 90$ ,  $m = 500$  GeV,  $x_F = 25$ .

The cases of  $\alpha = 0.1$  and  $\alpha = 0.2$  for Sommerfeld enhanced  $p$ -wave annihilation cross section are plotted in Fig.6 for kinetic decoupling temperatures  $x_k = 5x_F, 10x_F, 100x_F$ . Here  $\eta = 1 \times 10^{-12}$ ,  $m = 500$  GeV,  $a = 0$ ,  $b = 5 \times 10^{-25} \text{ cm}^3 \text{ s}^{-1}$ . Similar analysis with the  $s$ -wave annihilation can be done for the case of  $p$ -wave annihilation. The abundances for asymmetric Dark Matter particles are nearly not changed for different kinetic decoupling temperatures. For asymmetric Dark Matter anti-particle, the decrease of abundance is very small for  $\alpha = 0.1$  comparing to the case  $\alpha = 0.2$ . On the other hand, the decrease is larger for smaller inverse-scaled kinetic decoupling temperature  $x_k = 5x_F$  in the case when  $\alpha = 0.2$ . In panel (b), annihilations become insignificant at the point  $x_{\text{cut}} = 4.1 \times 10^5$  for  $x_k = 5x_F$ ,  $2.6 \times 10^5$  for  $x_k = 10x_F$  and  $6.9 \times 10^5$  for  $x_k = 100x_F$ .

The final relic abundance for asymmetric Dark Matter anti-particle for Sommerfeld enhanced  $s$ ,  $p$ -wave annihilations is obtained by integrating Boltzmann equation (19) from  $\bar{x}_F$  to  $x_k$  and equation (32) from  $x_k$  to  $x_{\text{cut}}$ , then

$$Y_{\bar{\chi}}(x_{\text{cut}}) = \eta \left\{ \exp \left[ 1.32 \eta m M_{\text{Pl}} \sqrt{g_*} \left( \int_{\bar{x}_F}^{x_k} \frac{\langle \sigma v \rangle_S}{x^2} dx + \int_{x_k}^{x_{\text{cut}}} \frac{\langle \sigma v \rangle_{S_k}}{x^2} dx \right) \right] - 1 \right\}^{-1}. \quad (33)$$

## 6 Constraints

Dark Matter relic density provided by Planck data [30] is

$$\Omega_{\text{DM}} h^2 = 0.1199 \pm 0.0022. \quad (34)$$

Fig.7 shows the contour plots of  $s$ - (panel (a)) and  $p$ -wave (panel (b)) annihilation cross sections and asymmetry factor  $\eta$  when  $\Omega_{\text{DM}} h^2 = 0.1199$ . The loosely dashed (red) line is for

the case of Sommerfeld enhancement without kinetic decoupling and dash dotted (black) line is for the case of kinetic decoupling when  $\alpha = 0.1$ , here the inverse-scaled kinetic decoupling temperature is  $x_k = 5x_F$ . The thick (red) line is for the case when there is no kinetic decoupling and the dotted (black) line is for inverse-scaled kinetic decoupling temperature  $x_k = 5x_F$  when  $\alpha = 0.2$ . We found the required annihilation cross section with kinetic decoupling is smaller than the case of without kinetic decoupling, i.e. when  $\alpha = 0.2$  and  $\eta = 1.0 \times 10^{-15}$  in panel (a), the required cross section is  $a = 5.99 \times 10^{-27} \text{ cm}^3 \text{ s}^{-1}$  for the case of kinetic decoupling and  $a = 7.20 \times 10^{-27} \text{ cm}^3 \text{ s}^{-1}$  for the case of no kinetic decoupling. The reason is that the relic density is decreased continuously after kinetic decoupling until the annihilation becomes inefficient. As a result there is less relic density for the case of kinetic decoupling comparing to the case of without kinetic decoupling. In order to satisfy the observed range of Dark Matter relic density, when there is kinetic decoupling, the annihilation cross section should be smaller than the case of without kinetic decoupling. On the other hand, the required annihilation cross section for  $\alpha = 0.2$  is two times smaller than the case of  $\alpha = 0.1$ . We can see the reason from Fig.5, the decrease of asymmetric Dark Matter anti-particle abundance is larger for larger coupling strength  $\alpha$ . Similar analysis can be done for the case of  $p$ -wave annihilation cross section in panel (b) in Fig.7, i.e. for  $\alpha = 0.2$  and  $\eta = 1.0 \times 10^{-15}$ , the required cross section is  $b = 6.35 \times 10^{-26} \text{ cm}^3 \text{ s}^{-1}$  for the case of kinetic decoupling and  $b = 6.80 \times 10^{-26} \text{ cm}^3 \text{ s}^{-1}$  for the case of no kinetic decoupling. The difference of the required cross section between the kinetic decoupling and no kinetic decoupling is very small for  $\alpha = 0.1$  for  $p$ -wave annihilation. We can find the reason from panel (a) and (b) of Fig.6. After kinetic decoupling, asymmetric Dark matter particle abundance is almost same for  $\alpha = 0.1$  and  $\alpha = 0.2$ . The decrease of anti-particle abundance for  $\alpha = 0.1$  is very small in panel (a) compared to the case of  $\alpha = 0.2$  in panel (b).

## 7 Summary and conclusions

We investigated the relic density of asymmetric Dark Matter which is coupled to the light force mediator. When the mediator is light enough, the interaction between the asymmetric Dark Matter particle and anti-particle is emerged as long-range interaction which distorts the wavefunction of two incoming asymmetric Dark Matter particle and anti-particle. It is indeed the Sommerfeld effect which enhances the annihilation rate of asymmetric Dark Matter at low velocity. The relic density of asymmetric Dark Matter is explored when the annihilation cross section is boosted by the Sommerfeld effect. First, we found the thermal average of Sommerfeld enhanced annihilation cross section. Then we derive the analytic formulae for relic abundances of asymmetric Dark Matter particle and anti-particle. We found the abundance for asymmetric

Dark Matter particle is not affected too much. On the other hand, the decrease of the relic abundance of asymmetric Dark Matter anti-particle is more obvious than the particle due to the Sommerfeld enhancement. The size of decrease depends on the Sommerfeld factor  $\alpha$ . For larger  $\alpha$ , there is sizable decrease of the relic abundance.

Then, we discuss the effects of kinetic decoupling on the relic abundances of asymmetric Dark Matter particle and anti-particle when the annihilation cross section of asymmetric Dark Matter is changed by the Sommerfeld effect. After chemical decoupling, the asymmetric Dark Matter particles and anti-particles continue to keep in kinetic equilibrium. When the scattering rate falls below the expansion rate of the universe, asymmetric Dark Matter particles and anti-particles decouple from kinetic equilibrium. The temperatures of asymmetric Dark Matter are different before and after kinetic decoupling. This leaves its imprint on the relic density of asymmetric Dark Matter particle and anti-particle. There is no effect on the  $s$ -wave annihilation while the impact is almost negligible for  $p$ -wave annihilation when there is no Sommerfeld enhancement. On the other hand, when the annihilation cross section is increased by the Sommerfeld enhancement, there are quite significant effects on relic density of asymmetric Dark Matter both for  $s$ - and  $p$ -wave annihilation cross sections.

In our work, we assumed that kinetic decoupling occurred after the chemical decoupling. The kinetic decoupling point is at least 5 times of the inverse-scaled freezing out temperature. We found the decrease is negligible for the abundance of asymmetric Dark Matter particle. The asymmetric Dark Matter anti-particle abundance is continuously decreased after the kinetic decoupling until the annihilations become insignificant. The magnitude of decrease depends on the size of kinetic decoupling temperature, the coupling strength  $\alpha$  and asymmetry factor  $\eta$ . The decrease is larger when the kinetic decoupling temperature is more close to the freezing out point. The reduction of anti-particle abundance is more sizable for larger  $\alpha$  and also for larger asymmetry factor  $\eta$ .

Finally, we used Planck data and found the constraints on annihilation cross section and asymmetry factor when there is kinetic decoupling and no kinetic decoupling. Our results show the required cross section for Dark Matter should be smaller than the case of without kinetic decoupling in order to fall in the observation range of Dark Matter relic density. It is because there is less relic density of asymmetric Dark Matter due to the kinetic decoupling. The result is important for determining the relic abundance of asymmetric Dark Matter when the Sommerfeld effect plays the role in low velocity. Sommerfeld effects imply the indirect detection signals from the annihilations of asymmetric Dark Matter anti-particle is significant. This provides us the possibility to probe the asymmetric Dark Matter with observations of the CMB (Cosmic Microwave Background), the Milky way and Dwarf galaxies.



# Acknowledgments

The work is supported by the National Natural Science Foundation of China (11765021).

# References

- [1] S. Nussinov, Phys. Lett. B **165**, (1985) 55; K. Griest and D. Seckel. Nucl. Phys. B **283**, (1987) 681; R. S. Chivukula and T. P. Walker, Nucl. Phys. B **329**, (1990) 445; D. B. Kaplan, Phys. Rev. Lett. **68**, (1992) 742; D. Hooper, J. March-Russell and S. M. West, Phys. Lett. B **605**, (2005) 228 [arXiv:hep-ph/0410114]; JCAP **0901** (2009) 043 [arXiv:0811.4153v1 [hep-ph]]; H. An, S. L. Chen, R. N. Mohapatra and Y. Zhang, JHEP **1003**, (2010) 124 [arXiv:0911.4463 [hep-ph]]; T. Cohen and K. M. Zurek, Phys. Rev. Lett. **104**, (2010) 101301 [arXiv:0909.2035 [hep-ph]]. D. E. Kaplan, M. A. Luty and K. M. Zurek, Phys. Rev. D **79**, (2009) 115016 [arXiv:0901.4117 [hep-ph]]; T. Cohen, D. J. Phalen, A. Pierce and K. M. Zurek, Phys. Rev. D **82**, (2010) 056001 [arXiv:1005.1655 [hep-ph]]; J. Shelton and K. M. Zurek, Phys. Rev. D **82**, (2010) 123512 [arXiv:1008.1997 [hep-ph]];
- [2] A. Belyaev, M. T. Frandsen, F. Sannino and S. Sarkar, Phys. Rev. D **83**, (2011) 015007 [arXiv:1007.4839].
- [3] M. L. Graesser, I. M. Shoemaker and L. Vecchi, JHEP **1110**, (2011) 110 [arXiv:1103.2771 [hep-ph]].
- [4] H. Iminniyaz, M. Drees and X. Chen, JCAP **1107**, (2011) 003 [arXiv:1104.5548 [hep-ph]].
- [5] A. Sommerfeld, Ann. Phys. **403** (1931) 257-330
- [6] M. Pospelov and A. Ritz, Phys. Lett. B **671** (2009), 391-397 doi:10.1016/j.physletb.2008.12.012 [arXiv:0810.1502 [hep-ph]].
- [7] J. D. March-Russell and S. M. West, Phys. Lett. B **676** (2009), 133-139 doi:10.1016/j.physletb.2009.04.010 [arXiv:0812.0559 [astro-ph]].
- [8] N. Arkani-Hamed, D. P. Finkbeiner, T. R. Slatyer and N. Weiner, Phys. Rev. D **79** (2009) 015014 doi:10.1103/PhysRevD.79.015014 [arXiv:0810.0713 [hep-ph]].
- [9] J. L. Feng, M. Kaplinghat and H. B. Yu, Phys. Rev. D **82** (2010) 083525 doi:10.1103/PhysRevD.82.083525 [arXiv:1005.4678 [hep-ph]].
- [10] M. Kamionkowski and S. Profumo, Phys. Rev. Lett. **101** (2008) 261301 doi:10.1103/PhysRevLett.101.261301 [arXiv:0810.3233 [astro-ph]].
- [11] J. B. Dent, S. Dutta and R. J. Scherrer, Phys. Lett. B **687** (2010) 275 doi:10.1016/j.physletb.2010.03.018 [arXiv:0909.4128 [astro-ph.CO]].

- [12] J. Zavala, M. Vogelsberger and S. D. M. White, Phys. Rev. D **81** (2010) 083502 doi:10.1103/PhysRevD.81.083502 [arXiv:0910.5221 [astro-ph.CO]].
- [13] J. L. Feng, M. Kaplinghat and H. B. Yu, Phys. Rev. Lett. **104** (2010) 151301 doi:10.1103/PhysRevLett.104.151301 [arXiv:0911.0422 [hep-ph]].
- [14] H. Imminiyaz and M. Kakizaki, Nucl. Phys. B **851** (2011) 57 doi:10.1016/j.nuclphysb.2011.05.009 [arXiv:1008.2905 [astro-ph.CO]].
- [15] I. Baldes and K. Petraki, JCAP **1709** (2017) 028 doi:10.1088/1475-7516/2017/09/028 [arXiv:1703.00478 [hep-ph]].
- [16] P. Agrawal, F. Y. Cyr-Racine, L. Randall and J. Scholtz, JCAP **1708** (2017) 021 doi:10.1088/1475-7516/2017/08/021 [arXiv:1702.05482 [astro-ph.CO]].
- [17] J. L. Feng, M. Kaplinghat, H. Tu and H. B. Yu, JCAP **0907** (2009) 004 doi:10.1088/1475-7516/2009/07/004 [arXiv:0905.3039 [hep-ph]].
- [18] K. Petraki, M. Postma and M. Wiechers, JHEP **1506** (2015) 128 doi:10.1007/JHEP06(2015)128 [arXiv:1505.00109 [hep-ph]].
- [19] T. Bringmann and S. Hofmann, JCAP **0704** (2007) 016 Erratum: [JCAP **1603** (2016) E02] doi:10.1088/1475-7516/2007/04/016, 10.1088/1475-7516/2016/03/E02 [hep-ph/0612238].
- [20] T. Bringmann, New J. Phys. **11** (2009) 105027 doi:10.1088/1367-2630/11/10/105027 [arXiv:0903.0189 [astro-ph.CO]].
- [21] H. Imminiyaz, X. L. Chen, X. J. Bi and S. Dulat, Commun. Theor. Phys. **56** (2011) 967. doi:10.1088/0253-6102/56/5/28
- [22] J. Hisano, M. Kawasaki, K. Kohri, T. Moroi, K. Nakayama and T. Sekiguchi, Phys. Rev. D **83** (2011) 123511 doi:10.1103/PhysRevD.83.123511 [arXiv:1102.4658 [hep-ph]].
- [23] J. Chen and Y. F. Zhou, JCAP **1304** (2013) 017 doi:10.1088/1475-7516/2013/04/017 [arXiv:1301.5778 [hep-ph]].
- [24] L. G. van den Aarssen, T. Bringmann and Y. C. Goedecke, Phys. Rev. D **85** (2012) 123512 doi:10.1103/PhysRevD.85.123512 [arXiv:1202.5456 [hep-ph]].
- [25] T. Binder, T. Bringmann, M. Gustafsson and A. Hryczuk, Phys. Rev. D **96** (2017) no.11, 115010 doi:10.1103/PhysRevD.96.115010 [arXiv:1706.07433 [astro-ph.CO]].
- [26] R. Iengo, JHEP **0905**, (2009) 024 [arXiv:0902.0688 [hep-ph]]; arXiv:0903.0317 [hep-ph].
- [27] R. J. Scherrer and M. S. Turner, Phys. Rev. D **33**, (1986) 1585, Erratum-ibid. D **34**, (1986) 3263.

- [28] X. l. Chen, M. Kamionkowski and X. m. Zhang, Phys. Rev. D **64** (2001), 021302  
doi:10.1103/PhysRevD.64.021302 [arXiv:astro-ph/0103452 [astro-ph]].
- [29] S. Hofmann, D. J. Schwarz and H. Stoecker, Phys. Rev. D **64** (2001), 083507  
doi:10.1103/PhysRevD.64.083507 [arXiv:astro-ph/0104173 [astro-ph]].
- [30] P. A. R. Ade *et al.* [Planck Collaboration], Astron. Astrophys. **594**, (2016) A13  
[arXiv:1502.01589 [astro-ph.CO]].